Recent Migration of Tropical Cyclones toward Coasts

S. Wang[1]*, R. Toumi[1]

[1]Department of Physics, Imperial College London, London, UK, SW7 2BU

*Correspondence to: shuai.wang@imperial.ac.uk

Abstract: Poleward migrations of tropical cyclones have been observed globally, but the impact on human and land exposure remains unclear. Here we investigate the change in global tropical cyclone activity in coastal regions over the period 1982-2018. We find that the distance of tropical cyclone maximum intensity to land has decreased by about 30 kilometers per decade. The annual frequency of global tropical cyclones increases with proximity to land by about two additional cyclones per decade. Trend analysis reveals a robust migration of tropical cyclone activity toward coasts, concurrently with poleward migration of cyclone locations, but more importantly, a larger and statistically significant westward shift. This zonal shift of tropical cyclone tracks may be mainly driven by global zonal changes in environmental steering flow.

One Sentence Summary: Geographical shifts of tropical cyclone track due to environmental condition changes lead to an increase in coastal storm activities.

Tropical cyclones are one of the most devastating natural disasters in terms of their average destructiveness and annual frequency affecting coastal regions. There are one-hundred-year records of tropical cyclone activity in some regions (*1, 2*), but only since 1982 have tropical cyclones been monitored globally by satellites. Poleward migration of the locations of tropical cyclone maximum intensity in the past 40 years has been reported in the global 'best-track' data (*3*), and projected to be continuing regionally in the twenty-first century (*4*). This poleward migration has been traced back to the poleward shift of tropical cyclone formation, which is speculated to be linked to an anthropogenically forced tropical circulation expansion (*5*). These trends could change the coastal tropical-cyclone risk in the future (*4*). However, the poleward migration of the locations of tropical cyclone formation and peak intensity by themselves may not necessarily indicate a change in coastal tropical cyclone risk directly, because these locations are commonly too far to generate an impact on the coasts. The change in coastal tropical cyclone activity and landfall frequency are a central and perhaps ultimate concern.

A tropical cyclone landfall is conventionally defined as the intersection of the surface center of a tropical cyclone with a coastline (*6*). To date, there has been no firm evidence of global trends of the frequency of tropical cyclones with maximum wind speed above the hurricane-force wind (64 knots) at landfall (*7*). However, a "near miss" or "indirect-hit" tropical cyclone track can also cause damage, for example, Sandy in 2012 and Dorian in 2019, skirted along the U.S. coast for a considerable time before making landfall. Investigating the trend of tropical cyclone entering coastal regions is therefore essential to better understand tropical cyclone risk.

Here we consider tropical cyclones, defined by the lifetime maximum intensity (LMI) reaching at least 34 knots (see Method), for a 37-year period 1982-2018. In this period, we have the most

confidence in data quality and its completeness in global basins (*8*). The poleward migration of tropical cyclone activity was first found at LMI (*3*). Here, we find that the annual-mean distance of the locations of LMI to the nearest land (Fig. 1a) also shows an evident and statistically significant decreasing trend of -32±31 km per decade (Table S1). The fraction of annual tropical cyclones entering coastal regions, defined as the offshore area with a distance to the nearest land less than 200 km (Fig. 1b), shows a robust increase of 2.2±1.9% per decade (Table S1). We also find positive trends of the annual-mean life-time fraction that tropical cyclones spend in coastal regions, at a statistically significant rate of 2.1±1.2% per decade globally, and in the Northern and Southern hemispheres of 2.1±1.6% and 2.1±1.9% per decade, respectively (Table S1). The consistently positive contribution from both hemispheres (Table S1) to the three global trends shown in Fig. 1 suggests that the increase of tropical cyclone activity in coastal regions is a global phenomenon, although regional differences between basins are evident.

The trend of the frequency of coastal tropical cyclones increases very significantly with proximity to land by one cyclone per decade per 1000 km (Fig. 2 and Table S2). There are about 2±2 additional tropical cyclones per decade in the 200-km coastal region globally (Fig. 2). Consistent with this, the fraction of annual tropical cyclones entering coastal regions (Fig. S1a), and the annual-mean life-time fraction that tropical cyclones spend in coastal regions (Fig. S1b) increase with proximity to land. The statistical significance remains by excluding short-lived storms (*9*) and using an alternative set of tropical cyclone records (Table S3). These clear increases in trend with reduced distance-to-land threshold suggest a global-scale landward migration of tropical cyclone activity.

Considering the geometry of global land-sea distribution, zonal and/or meridional shift of tropical cyclone locations may lead to a change of tropical cyclone activity in coastal regions. Our analysis shows that from 1982-1999 to 2000-2018 the epochal mean tropical cyclone location in the global basins is found to be migrating not only poleward, but also westward (Table 1). The globally epochal poleward and westward shifts are both statistically significant. If we measure the track shift in terms of degrees, the zonal shift is considerably larger than the meridional change. Tropical cyclone activity is being shifted westward in the West Pacific, East Pacific, North and South Indian Ocean. These four basins account for about 75% of global tropical cyclones for 1982-2018, which accounts for the global mean westward track shifts. There are eastward track shifts in the South Pacific, and no significant zonal shifts in the North Atlantic. These basin-wise changes in tropical cyclone locations can also be seen in the density change of tropical cyclone locations between the two epochs (Fig. S2).

We do not find any statistically significant global change in cyclone zonal translation velocity, duration or zonal shifts of cyclone genesis (Table S4). The lack of regionally significant zonal genesis location change is different from a reported poleward shift of genesis in the Pacific Ocean basins (*10*). The relative changes in meridional cyclone translation velocity in the second epoch agree with the meridional track shifts in all the basins. Tropical cyclone tracks are primarily determined by the environmental steering flow and genesis location (*11*, *12*).We find significant enhancement of westward steering at a global scale in all basins except the North Indian Ocean (Table 1). Consistent general circulation patterns are confirmed in all three reanalysis products (Fig. S3a-c). The global mean change in zonal steering (+0.3 m s^{-1}, Table 1) is about 11% of the global mean zonal steering speed (2.6 m s^{-1} in ERA5 reanalysis, Fig. S3) and global mean cyclone zonal translation speed (2.7 m s^{-1}). The West Pacific, East Pacific and South Indian Ocean show both westward track shift and enhanced westward environmental steering

between the epochs. The West Pacific is the only basin that shows a consistent link between the seasonal westward steering enhancement, larger westward cyclone velocity and westward track shift. This only robust linkage to seasonal mean environmental conditions may be due to the considerably larger fraction of storm days in the season in the West Pacific compared to the other basins (*13*).

An environment with reduced vertical wind shear and/or increased potential intensity are favorable for tropical cyclone development (*14*, *15*) and may also contribute to geographical shifts of tropical cyclone locations (*3*). We find a significantly relative decrease in vertical wind shear from the east to west globally (Fig. 3), which is confirmed in individual basins with reanalysis products (Fig. S4a-f). The South Pacific is the only basin where neither steering flow nor the vertical wind shear fully explain the regional eastward track shift. However, we do find a relative increase in potential intensity to the east and a decrease to the west in that basin (Fig. S4l). In the North Atlantic the shear weakens only in the central part of the basin (Fig. S4c) with no zonal change in either steering (Table 1) or potential intensity (Fig. S4i), which is consistent with also no significant zonal track shift. Further analysis reveals that the zonal potential intensity change is primarily modulated by the variation of the atmospheric convective available potential energy (Fig. S5).

Given the dominant role of steering flow in tropical cyclone tracks (*12*) and a larger epochal relative change of steering (Table 1) than wind shear (Fig. 3) in our analysis, it is very likely that the westward shift of cyclone tracks is mainly due to the enhanced westward steering. Anomalous westward steering may increase tropical cyclone frequency in the West of the basins and relatively reduced vertical wind shear provides a further favorable environment for cyclones there. The quantitative contribution of the three environmental factors needs further exploration. Climate modes such as the El Niño/Southern Oscillation (ENSO) and Pacific Decadal Oscillation (PDO), considered as measures of mainly internal unforced variability, can modulate tropical cyclone activities (*16*–*19*) and global atmospheric circulation in the tropics (*20*, *21*). We find very limited impact of ENSO on annual trends. However, the PDO could substantially contribute to the trends in the Northern Hemisphere (Table S1). The epochal steering flow change is similar to the steering difference between PDO warm and cold phases (Fig. S3d-f). The PDO index had a phase change in 1998 (*5*) which also separates the first and second epochs (pre and post 2000) in our analysis into a warm and cold PDO phase, respectively.

Given no strong trend of global annual frequency of tropical cyclones (*22*), an increasing trend of annual coastal cyclone fraction agrees with a rising frequency of coastal tropical cyclones shown here. The lifetime fraction trend in Fig. 1c seems to agree with a recently reported global slowdown of tropical cyclone translation speed (*23*) since the annual-mean tropical cyclone duration has not changed significantly during the period 1982-2018 (Table S4). However, this causal hypothesis needs to be confirmed as changes in cyclone moving speed are disputed (*24*).

We find statistically significant landward migration of tropical cyclone activity. The lack of a statistically significant trend of actual landfall (+1±2 cyclones per decade globally) may be due to the rapid intensity reduction prior to and during landfall. Major tropical cyclones have decayed more rapidly post LMI (*25*). This could stabilize the annual frequency of landfall defined by a fixed intensity threshold. Thus, the lack of global trend of annual mean landfall frequency, as has been previously reported (*7*) and confirmed in our analysis, may not be contradictory to the increase in tropical cyclone activity in coastal regions reported here.

Long-term zonal migration of tropical cyclones as found in our analysis has been previously shown directly or indirectly in some individual basins for different metrics. In the West Pacific, westward migration of the tropical cyclone maximum intensity locations was reported (*26*), which was related to the strengthened tropical Pacific Walker circulation driven by the zonally enhanced sea surface temperature gradient. No detectable trend of the U.S. landfalling-hurricane frequency has emerged (*22*). There has been a decreasing trend of landfall frequency by severe tropical cyclones in the eastern Australia (*2*). In the North Indian Ocean, the reduction of local wind shear over the Arabian Sea has made tropical cyclone development more favorable and this may continue in the future (*27*).

The relatively limited length of global tropical cyclone observations, limitations of climate modelling and possible association with the PDO limit our ability to attribute tropical cyclone migration toward coasts to anthropogenic forcing. However, we note that global epochal westward shifts are still present when considering only PDO neutral years (Table S5). The West Pacific LMI distance to land, fraction of coastal cyclones, and coastal time fraction trends since 1950 are still significant after the PDO removal (Table S1). This suggests factors other than the PDO are also important. It is argued that greenhouse gas emissions have contributed to the observed changes in regional distribution of tropical cyclones since 1980, and yet these trends may not persist in the 21st century (*28*).

The enhanced westward tropical cyclone steering may also be consistent with Hadley circulation expansion. The phase change in PDO and Hadley circulation expansion are related (*20*, *21*). The poleward migration of cyclone locations has also been related to the anomalous sinking and rising motions due to the meridional expansion of the Hadley circulation (*5*). Long-term zonal shifts of tropical precipitation emerge in atmospheric re-analysis data (*29*). The Walker circulation dominates the large-scale zonal motion in the tropics. An attempt has been made to establish a link between the co-variability of tropical cyclone genesis locations with both the Hadley and Walker circulations in the West Pacific (*30*). The combined Walker and Hadley circulation variation is a plausible avenue for future study to understand the global tropical cyclone changes presented here. Given the considerable impacts of coastal tropical cyclones, further study of the changes in coastal tropical cyclone activity, as identified here, and its future projections and the consequent risk change, is warranted.

References and Notes:

1. J. C. L. Chan, K.-S. Liu, M. Xu, Q. Yang, Variations of frequency of landfalling typhoons in East China, 1450-1949. *Int. J. Climatol.* **32**, 1946–1950 (2012).

2. J. Callaghan, S. B. Power, Variability and decline in the number of severe tropical cyclones making land-fall over eastern Australia since the late nineteenth century. *Clim. Dyn.* **37**, 647–662 (2011).

3. J. P. Kossin, K. A. Emanuel, G. A. Vecchi, The poleward migration of the location of tropical cyclone maximum intensity. *Nature*. **509**, 349–352 (2014).

4. J. P. Kossin, K. A. Emanuel, S. J. Camargo, Past and projected changes in western north

pacific tropical cyclone exposure. *J. Clim.* **29**, 5725–5739 (2016).

5. S. Sharmila, K. J. E. Walsh, Recent poleward shift of tropical cyclone formation linked to Hadley cell expansion. *Nat. Clim. Chang.* **8**, 730–736 (2018).

6. Glossary of National Hurricane Center Terms. Accessed on 16 Feburary 2020., (available at https://www.nhc.noaa.gov/aboutgloss.shtml).

7. J. Weinkle, R. Maue, R. Pielke, Historical global tropical cyclone landfalls. *J. Clim.* **25**, 4729–4735 (2012).

8. K. R. Knapp, M. C. Kruk, Quantifying interagency differences in tropical cyclone best-track wind speed estimates. *Mon. Weather Rev.* **138**, 1459–1473 (2010).

9. C. W. Landsea, G. A. Vecchi, L. Bengtsson, T. R. Knutson, Impact of duration thresholds on Atlantic tropical cyclone counts. *J. Clim.* **23**, 2508–2519 (2010).

10. A. S. Daloz, S. J. Camargo, Is the poleward migration of tropical cyclone maximum intensity associated with a poleward migration of tropical cyclone genesis? *Clim. Dyn.* **50**, 705–715 (2018).

11. L. Wu, B. Wang, Assessing Impacts of Global Warming on Tropical Cyclone Tracks*. *J. Clim.* **17**, 1686–1698 (2004).

12. J. C. L. Chan, the Physics of Tropical Cyclone Motion. *Annu. Rev. Fluid Mech.* **37**, 99–128 (2005).

13. B. Wang, Y. Yang, Q. H. Ding, H. Murakami, F. Huang, Climate control of the global tropical storm days (1965–2008). *Geophys. Res. Lett.* **37**, 1–5 (2010).

14. K. A. Emanuel, Thermodynamic control of hurricane intensity. *Nature*. **401**, 665–669 (1999).

15. M. Ting, J. P. Kossin, S. J. Camargo, C. Li, Past and Future Hurricane Intensity Change along the U.S. East Coast. *Sci. Rep.* **9**, 1–8 (2019).

16. S. J. Camargo, A. W. Robertson, A. G. Barnston, M. Ghil, Clustering of eastern North Pacific tropical cyclone tracks: ENSO and MJO effects. *Geochemistry, Geophys. Geosystems*. **9** (2008), doi:10.1029/2007GC001861.

17. J. P. Kossin, S. J. Camargo, M. Sitkowski, Climate modulation of north atlantic hurricane tracks. *J. Clim.* **23**, 3057–3076 (2010).

18. S. J. Camargo, A. W. Robertson, S. J. Gaffney, P. Smyth, M. Ghil, Cluster analysis of typhoon tracks. Part II: Large-scale circulation and ENSO. *J. Clim.* **20**, 3654–3676 (2007).

19. H. A. Ramsay, S. J. Camargo, D. Kim, Cluster analysis of tropical cyclone tracks in the Southern Hemisphere. *Clim. Dyn.* **39**, 897–917 (2012).

20. R. J. Allen, M. Kovilakam, The Role of Natural Climate Variability in Recent Tropical Expansion. *J. Clim.* **30**, 6329–6350 (2017).

21. P. W. Staten, J. Lu, K. M. Grise, S. M. Davis, T. Birner, Re-examining tropical expansion. *Nat. Clim. Chang.* **8**, 768–775 (2018).

22. T. Knutson, S. J. Camargo, J. C. L. Chan, K. Emanuel, C.-H. Ho, J. Kossin, M. Mohapatra, M. Satoh, M. Sugi, K. Walsh, L. Wu, Tropical Cyclones and Climate Change

Assessment: Part I: Detection and Attribution. *Bull. Am. Meteorol. Soc.* **100**, 1987–2007 (2019).

23. J. P. Kossin, A global slowdown of tropical-cyclone translation speed. *Nature*. **558**, 104–107 (2018).
24. M. Yamaguchi, J. C. L. Chan, I. J. Moon, K. Yoshida, R. Mizuta, Global warming changes tropical cyclone translation speed. *Nat. Commun.* **11**, 1–7 (2020).
25. S. Wang, T. Rashid, H. Throp, R. Toumi, A Shortening of the Life Cycle of Major Tropical Cyclones. *Geophys. Res. Lett.* **47** (2020), doi:10.1029/2020GL088589.
26. D.-S. R. Park, C.-H. Ho, J.-H. Kim, Growing threat of intense tropical cyclones to East Asia over the period 1977–2010. *Environ. Res. Lett.* **9**, 014008 (2014).
27. H. Murakami, G. A. Vecchi, S. Underwood, Increasing frequency of extremely severe cyclonic storms over the Arabian Sea. *Nat. Clim. Chang.* **7**, 885–889 (2017).
28. H. Murakami, T. L. Delworth, W. F. Cooke, M. Zhao, B. Xiang, P. C. Hsu, Detected climatic change in global distribution of tropical cyclones. *Proc. Natl. Acad. Sci. U. S. A.* **117**, 10706–10714 (2020).
29. M. P. Byrne, A. G. Pendergrass, A. D. Rapp, K. R. Wodzicki, Response of the Intertropical Convergence Zone to Climate Change: Location, Width, and Strength. *Curr. Clim. Chang. Reports*. **4**, 355–370 (2018).
30. H. Zhao, J. Zhang, P. J. Klotzbach, S. Chen, Recent Increased Covariability of Tropical Cyclogenesis Latitude and Longitude over the Western North Pacific during the Extended Boreal Summer. *J. Clim.* **32**, 8167–8179 (2019).
31. K. R. Knapp, M. C. Kruk, D. H. Levinson, H. J. Diamond, C. J. Neumann, The International Best Track Archive for Climate Stewardship (IBTrACS). *Bull. Am. Meteorol. Soc.* **91**, 363–376 (2010).
32. Copernicus Climate Change Service (C3S) (2017): ERA5: Fifth generation of ECMWF atmospheric reanalyses of the global climate . Copernicus Climate Change Service Climate Data Store (CDS), accessed on 16 Feb 2020., (available at https://cds.climate.copernicus.eu/cdsapp#!/home).
33. M. M. Rienecker, M. J. Suarez, R. Gelaro, R. Todling, J. Bacmeister, E. Liu, M. G. Bosilovich, S. D. Schubert, L. Takacs, G.-K. Kim, S. Bloom, J. Chen, D. Collins, A. Conaty, A. da Silva, W. Gu, J. Joiner, R. D. Koster, R. Lucchesi, A. Molod, T. Owens, S. Pawson, P. Pegion, C. R. Redder, R. Reichle, F. R. Robertson, A. G. Ruddick, M. Sienkiewicz, J. Woollen, MERRA: NASA's Modern-Era Retrospective Analysis for Research and Applications. *J. Clim.* **24**, 3624–3648 (2011).
34. E. Kalnay, M. Kanamitsu, R. Kistler, W. Collins, D. Deaven, L. Gandin, M. Iredell, S. Saha, G. White, J. Woollen, Y. Zhu, A. Leetmaa, R. Reynolds, M. Chelliah, W. Ebisuzaki, W. Higgins, J. Janowiak, K. C. Mo, C. Ropelewski, J. Wang, R. Jenne, D. Joseph, The NCEP/NCAR 40-Year Reanalysis Project. *Bull. Am. Meteorol. Soc.* **77**, 437–471 (1996).
35. D. S. Wilks, *Statistical methods in the atmospheric sciences* (Academic press, 2011), vol. 100.

36. K. Emanuel, Sensitivity of Tropical Cyclones to Surface Exchange Coefficients and a Revised Steady-State Model Incorporating Eye Dynamics. *J. Atmos. Sci.* **52**, 3969–3976 (1995).

37. A. G. Barnston, M. Chelliah, S. B. Goldenberg, Documentation of a highly ENSO-related sst region in the equatorial pacific: Research note. *Atmosphere-Ocean*. **35**, 367–383 (1997).

38. K. Ashok, S. K. Behera, S. A. Rao, H. Weng, T. Yamagata, El Niño Modoki and its possible teleconnection. *J. Geophys. Res. Ocean.* **112**, 1–27 (2007).

39. Yuan Zhang, J. M. Wallace, D. S. Battisti, ENSO-like interdecadal variability: 1900-93. *J. Clim.* **10**, 1004–1020 (1997).

40. N. J. Mantua, S. R. Hare, Y. Zhang, J. M. Wallace, R. C. Francis, A Pacific Interdecadal Climate Oscillation with Impacts on Salmon Production. *Bull. Am. Meteorol. Soc.* **78**, 1069–1079 (1997).

Acknowledgments

We thank C. Landsea, two anonymous reviewers and K. Emanuel for helpful comments. **Funding:** This work was supported by the UK-China Research and Innovation Partnership Fund through the Met Office Climate Science for Service Partnership (CSSP) China as part of the Newton Fund. **Author contributions:** S.W. and R.T. conceived the study. S.W. performed the analysis. Both the authors discussed the results and jointly contributed to writing the manuscript. **Competing interests:** The authors declare no competing interests. **Data and materials availability:** The tropical cyclone best track data can be downloaded from the National Centers for Environmental Information website (https://www.ncdc.noaa.gov/ibtracs/index.php). The ERA5, MERRA and NCEP/NCAR reanalysis data are available at the European Centre for Medium-Range Weather Forecasts (https://www.ecmwf.int/en/forecasts/datasets/reanalysis-datasets/era5), the Modeling and Assimilation Data and Information Services Center (https://gmao.gsfc.nasa.gov/reanalysis/MERRA-2/), and the Physical Sciences Laboratory (https://psl.noaa.gov/data/reanalysis/reanalysis.shtml), respectively.

Supplementary Materials:

Materials and Methods

Figures S1-S6

Tables S1-S5

Reference (*31-40*)

Table 1. Changes in mean tropical cyclone location and deep-layer steering flow between periods 2000-2018 to 1982-1999. The seasonal mean steering flow is calculated with ERA5 re-analysis product. The meridional steering flow is not shown since the absolute mean epochal change is less than 0.1 m s^{-1} in all regions. Statistical significance is indicated in bold at the 95% confidence interval. The differences are calculated globally, in the hemispheres (NHEM, Northern Hemisphere; SHEM, Southern Hemisphere) and in the individual basins (NATL, North Atlantic; WPAC, West Pacific; EPAC, East Pacific; NIO North Indian Ocean; SIO, South Indian Ocean; SPAC, South Pacific).

	Global	NHEM	SHEM	WPAC	EPAC	NATL	NIO	SIO	SPAC
Westward (degree longitude)	**+0.8±0.2**	**+1.0±0.3**	**+0.4±0.3**	**+1.6±0.4**	**+1.3±0.7**	–0.1±0.5	**+2.7±0.4**	**+1.4±0.5**	**–1.6±0.6**
Poleward (degree latitude)	**+0.3±0.1**	**+0.2±0.1**	**+0.6±0.2**	**+0.5±0.2**	**+0.4±0.2**	**–0.3±0.3**	**–0.8±0.3**	**+0.6±0.2**	**+0.5±0.3**
Zonal steering (m s^{-1})	**+0.3±0.3**	+0.2±0.3	+0.4±0.6	**+0.4±0.4**	**+0.4±0.3**	+0.1±0.3	–0.1±0.3	+0.3±0.5	+0.5±0.7

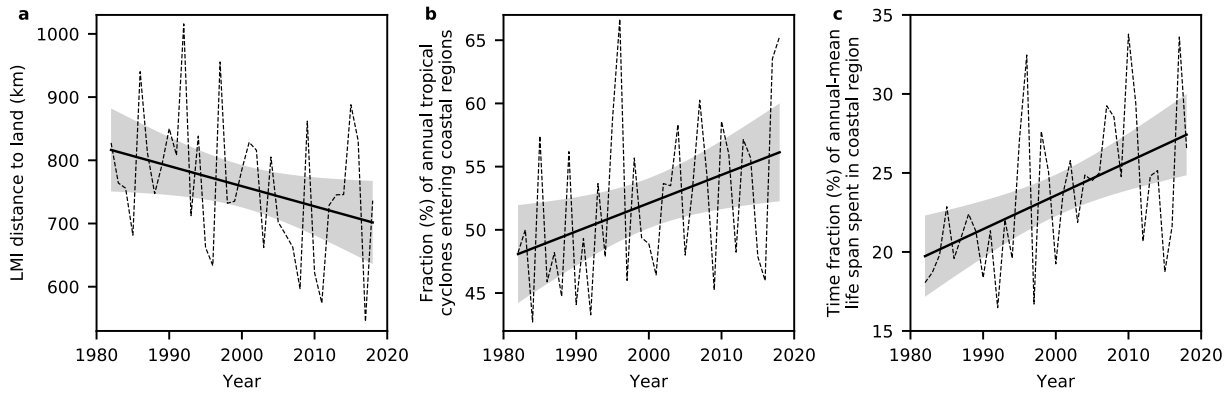

Fig. 1. Landward migration of global tropical cyclone activity. a, the time series of annual-mean distance to land of the locations of lifetime maximum intensity (LMI). b, as in a, but for the fraction of annual tropical cyclones entering coastal regions. c, as in a, but for the time fraction of annual-mean life span spent in coastal regions. The dashed lines show the historical data. The solid lines show the linear trends. The shadings represent the 95% confidence interval of the linear trend.

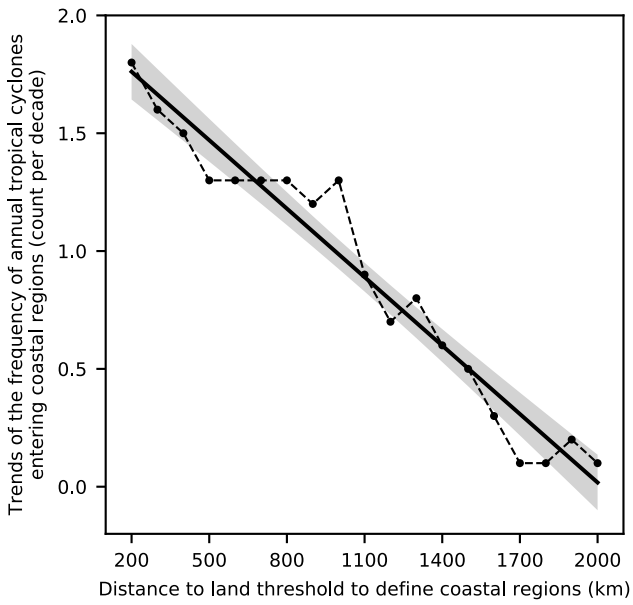

Fig. 2. Increasing trend of global tropical cyclone activity in coastal regions when reducing the distance-to-land threshold for coastal region definition. Changes in trends of the frequency of global annual tropical cyclones entering coastal regions by reducing the distance-to-land threshold from 2000 km to 200 km at every 100-km interval. The dashed line, solid line and shading show the historical data, linear trend and 95% confidence interval of the trend, respectively. On average there are 45 cyclones per year reaching coastal regions within 200 km to land.

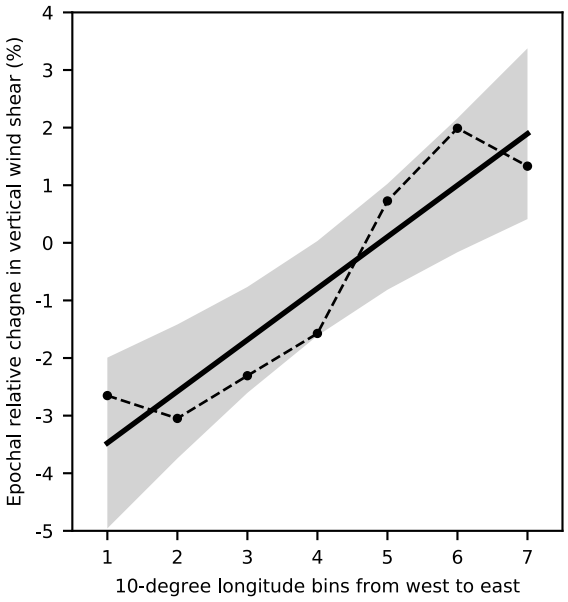

Figure 3. Epochal change in the global-mean basin-wise climate condition as a function of longitude. The climate condition shown here is calculated as the relative change in vertical wind shear in the second epoch 2000-2018 with respect to that in the first epoch 1982-1999. The vertical wind shear is extracted from the reanalysis product ERA5. The mean vertical wind shear is calculated in seven of the 10-degree longitude bins, from west to east, in all the basins. The black dashed line shows the mean relative change in the seven longitude bins. The solid line shows the linear fit with the ordinary least squares regression. The shading represents the 95% confidence interval of the fit.

Science
AAAS

Supplementary Materials for

Recent Migration of Tropical Cyclones toward Coasts

S. Wang[1]*, R. Toumi[1]

[1]Department of Physics, Imperial College London, London, UK, SW7 2BU

*Correspondence to: shuai.wang@imperial.ac.uk

This PDF file includes:

Materials and Methods

Data

Best-track data were taken from the International Best Track Archive for Climate Stewardship (IBTrACS) v04r00 (*31*). We chose the best-track archive from the National Hurricane Center and Joint Typhoon Warming Center, respectively, to cover the East Pacific (EPAC) and North Atlantic (NATL), and the West Pacific (WPAC), North Indian Ocean (NIO), South Indian Ocean (SIO) and South Pacific (SPAC). In this IBTrACS version, the distance to the nearest land, including all continents and any islands larger than 1400 km^2 (equivalent to the area of Kauai, Hawaii), is provided for each best-track geographical location. The best-track data provided by the World Meteorological Organization agencies in the IBTrACS were also used to cross check the main findings. Three monthly-mean reanalysis products, ERA5 (*32*), MERRA (*33*) and NCEP/NCAR (*34*), are used to extract climate variables for 1982-2018. In satellite era we have more confidence in the reanalysis variables over the ocean.

Tropical cyclone selection

Firstly, we only kept the best-track data at the regular 6-hour intervals, i.e., 00, 06, 12 and 18 Universal Time Coordinates. Secondly, for each cyclone we excluded locations outside 40^{o}N-40^{o}S to reduce the sub-tropical impact. Thirdly, we excluded a tropical cyclone case if its lifetime maximum intensity is less than 34 knots. Finally, we kept the offshore best-track data with an intensity of at least 34 knots and only the first record after landfall when the distance to land parameter becomes 0 km. The full tracks of tropical cyclones with the LMI of at least 34 knots over the period 1982-2018 (blue lines) and the selected partial tracks used in our analysis (red lines) are shown in Fig. S6.

Epochal changes in tropical cyclone locations and translation velocity

Firstly, we calculated a pair of latitude and longitude coordinate in each basin, by taking the mean of all cyclone positions for 1982-2018. This coordinate was then the reference point in the basin. Secondly, the latitude and longitude of all the tropical cyclone tracks in a basin were normalized by subtracting the reference point of that basin. By doing so, the tropical cyclones in different basins can be combined to calculate meridional and zonal changes in the two epochs globally, and in both hemispheres. Similarly, we calculate the epochal mean translation velocity at all positions of all the tracks, rather than the tropical cyclone mean velocity of a track. The period mean difference between 2000-2018 and 1982-1999 was taken as the epochal change.

Change detection and statistical significance

We examined the change of tropical cyclone coastal activity by linear trend analysis, and the mean difference analysis in the two epochs. Both methods have been used previously to investigate the migration of tropical cyclone locations (*3,5,23*). The statistical significance was evaluated with 95% confidence intervals (CIs).

For the linear trend analysis, ordinary least-squares regression was used. The CIs of the estimated linear trend were calculated from the standard error of the linear fit and degrees of

freedom. We tested for autocorrelation with the Durbin-Watson test for AR(1). If an AR(1) process was detected, the CIs were then calculated after adjusting degrees of freedom with the lag-1 autocorrelation coefficient (*35*).

For the analysis based on the two epochs, we chose two-sided bootstrapping to calculate the CIs, considering the tested populations are not necessarily normally distributed. Two bootstrapping methods are used:

1. Tropical cyclone track and translation velocity (Table 1, S3, S4 and S5)

   The observed populations in two epochs consist of independent time series of individual cyclones. These time series had autocorrelation, AR(1), so the "moving-blocks bootstrap" method (*35*) was applied for each time series. We could thereby avoid destroying the ordering that produces the autocorrelation. Difference of the new means in the two epochs was calculated. We then repeated the last two steps 100,000 times to generate a resampled distribution containing 100,000 estimates of the mean epochal difference. To get the 95% CIs, we extracted the 2.5th and 97.5th percentiles of the new resampled distribution from the last step as the CI bounds.

2. Tropical cyclone genesis locations and duration and steering flow (Table 1 and S3)

   The observed populations in two epochs consist of independent observations. We resampled 100,000 times the two tested populations directly to generate 100,000 pairs of two distributions. The difference of the means between the resampled distributions in each pair was calculated to form a difference distribution that was used to obtain the 95% CIs.

Environmental variables

The deep-layer steering flow was calculated with zonal and meridional wind velocities averaged across pressure levels of 300, 400, 500, 600, 700 and 800 hPa. The vertical wind shear was calculated as the amplitude of wind vector difference between 200- and 850-hPa pressure levels. The potential intensity (PI) was obtained as (*36*):

$$PI = \alpha\sqrt{\frac{C_K}{C_D}} \cdot \sqrt{\frac{1}{T_o}} \cdot \sqrt{T_s} \cdot \sqrt{(CAPE_s - CAPE)} \quad (1)$$

where C_K is the exchange coefficient for enthalpy, C_D is the drag coefficient, T_S is the sea surface temperature, T_o is the outflow temperature, $CAPE_s$ is the convective available potential energy of saturated air lifted from the sea level via the environmental sounding, and $CAPE$ is that of boundary layer air. The parameter α represents the wind speed reduction from the top of boundary layer to near-surface level, which was conventionally set to 0.8. The ratio of C_K to C_D was fixed to 0.9 by default.

The deep-layer steering flow, vertical wind shear and potential intensity were calculated in the region spanning latitude 10-35ºN and averaged over August-October in the North Hemisphere, and 10-35ºS over January-March in the South Hemisphere. A 70-degree longitude window was applied in each basin as shown in Fig. S3. The deep-layer steering flow was averaged in each basin within the 25-degree-latitude by 70-degree-longitude box. The vertical wind shear and

potential intensity were averaged in seven 10-degree meridional bins in each basin to obtain the zonal climate condition profiles (Fig. S4).

The steering flow, vertical wind shear and potential intensity were calculated over water only.

Climate indices removal

Two kinds of climate indices were considered, i.e., ENSO (Canonical Type and Modoki Type) and PDO. Canonical ENSO variability was represented by the Niño-3.4 index (*37*). The indices of ENSO Modoki and PDO were calculated according to reference (*38*) and (*39*, *40*), respectively. Climate variability time series were averaged over August-October in the North Hemisphere and January-March in the South Hemisphere.

To reduce the potential contribution of climate variability in the linear trend analysis, we analyzed the trends of the residuals from the regression of the original time series onto the climate oscillation index. Regarding the epochal changes, we performed the analysis with the PDO neutral years (Table S5). A neutral year in one hemisphere is identified when the corresponding summer PDO index is between -0.5^{o}C and +0.5^{o}C. There are 13 and 11 PDO neutral years in the North and South Hemispheres, respectively, in the period 1982-2018.

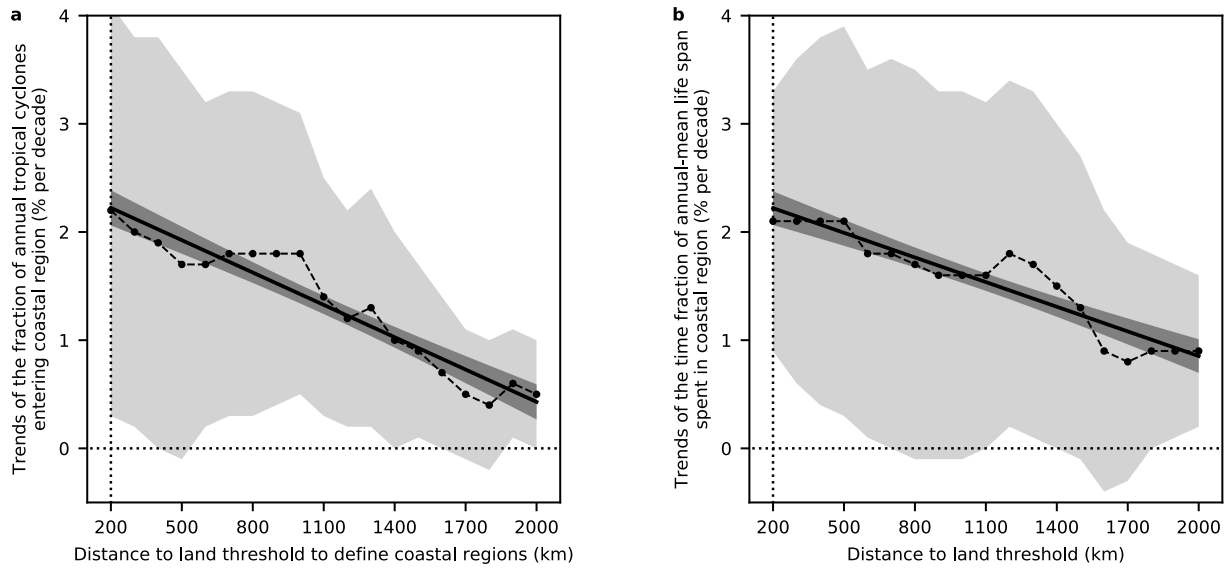

Fig. S1. As in Fig. 2, but for changes in trends of (a) the fraction of global annual tropical cyclones entering coastal regions. b, as in a, but for the time fraction of global annual-mean tropical cyclone life span spent in coastal regions. The extra light grey shading shows the 95% confidence interval of the trend with a given distance-to-land threshold for coastal region definition.

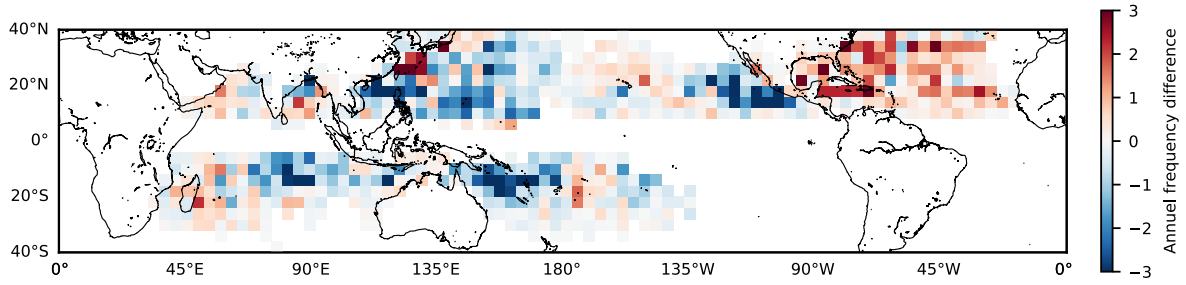

Fig. S2. Annual tropical cyclone frequency difference between the two epochs (2000-2018 and 1982-1999). A positive difference means an increase in cyclone frequency in the second epoch. The frequency is calculated in every 4-degree longitude by 4-degree latitude box. Annual trends in the East Pacific (Table S1) are partly due to closer approach of the Hawaii Islands.

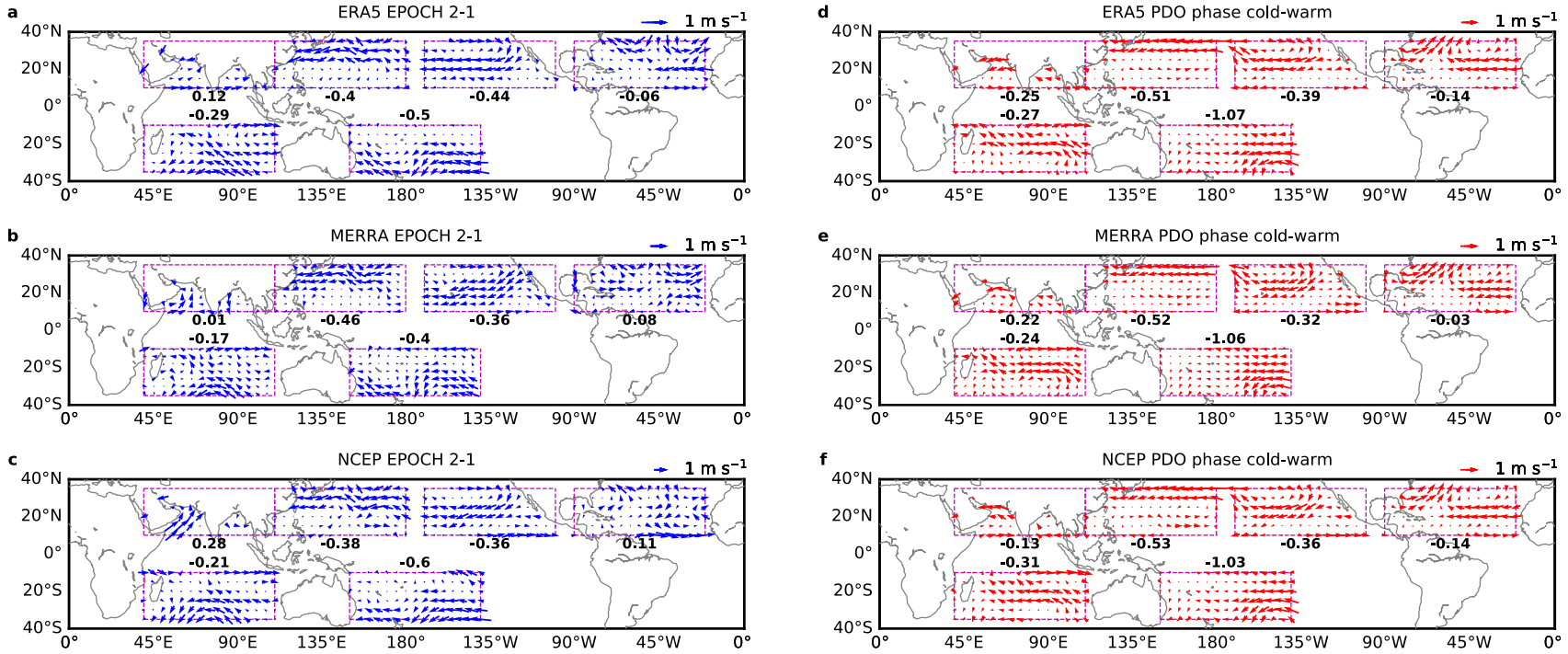

Fig. S3. Deep-layer seasonal-mean steering flow changes for the period 1982-2018. a-c, epochal changes. d-f, changes between PDO cold and warm phases. Three reanalysis products are used: ERA5 (a, d), MERRA (b, e) and NCEP/NCAR (c, f). The steering flow is averaged between 300 and 800 hPa, over August-October in the North Hemisphere and January-March in the South Hemisphere. Each basin is covered by a 70-degree-longtitude by 25-degree-latitude box. The latitude range is 10ºN/S-35ºN/S for North/South Hemisphere, respectively. The mean zonal steering change is given in each basin with unit of m s^{-1}. The global mean zonal steering speed is 2.6, 2.8, and 2.9 m s^{-1} in ERA5, MERRA, and NCEP/NCAR reanalysis, respectively.

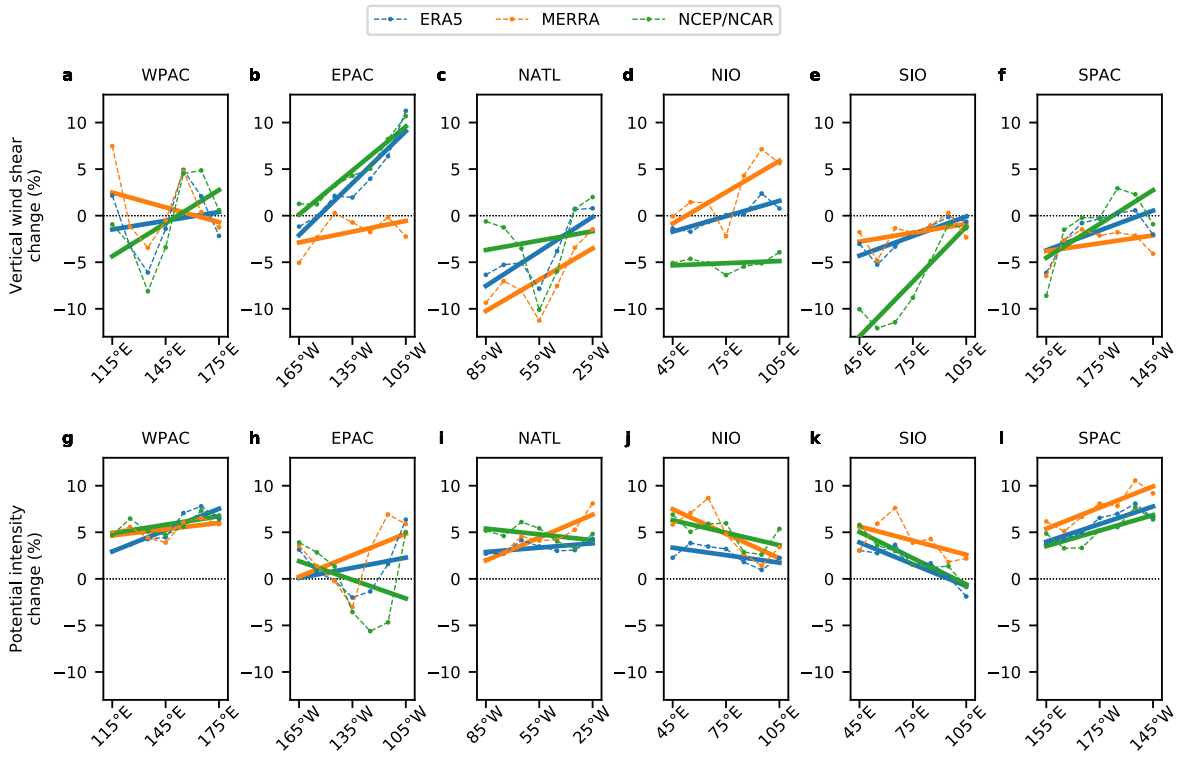

Fig. S4. Epochal changes, by basin, in seasonal-mean large-scale climate conditions as a function of longitude. a-f, relative change in vertical wind shear in the second epoch 1982-1999 with respect to that in the first epoch 2000-2018. g-l, as in a-f, but for the potential intensity. Three reanalysis products are used: ERA5, MERRA and NCEP/NCAR. The seasonal mean conditions are averaged over August-October in the North Hemisphere and January-March in the South Hemisphere. Each basin is covered by seven 10-degree-longtitude bins, and the latitude range is 10ºN/S-35ºN/S for North/South Hemisphere, respectively. The calculation area in each basin is shown in Fig. S3. The thick solid line shows the linear fit of zonal variation using the ordinary least squares regression.

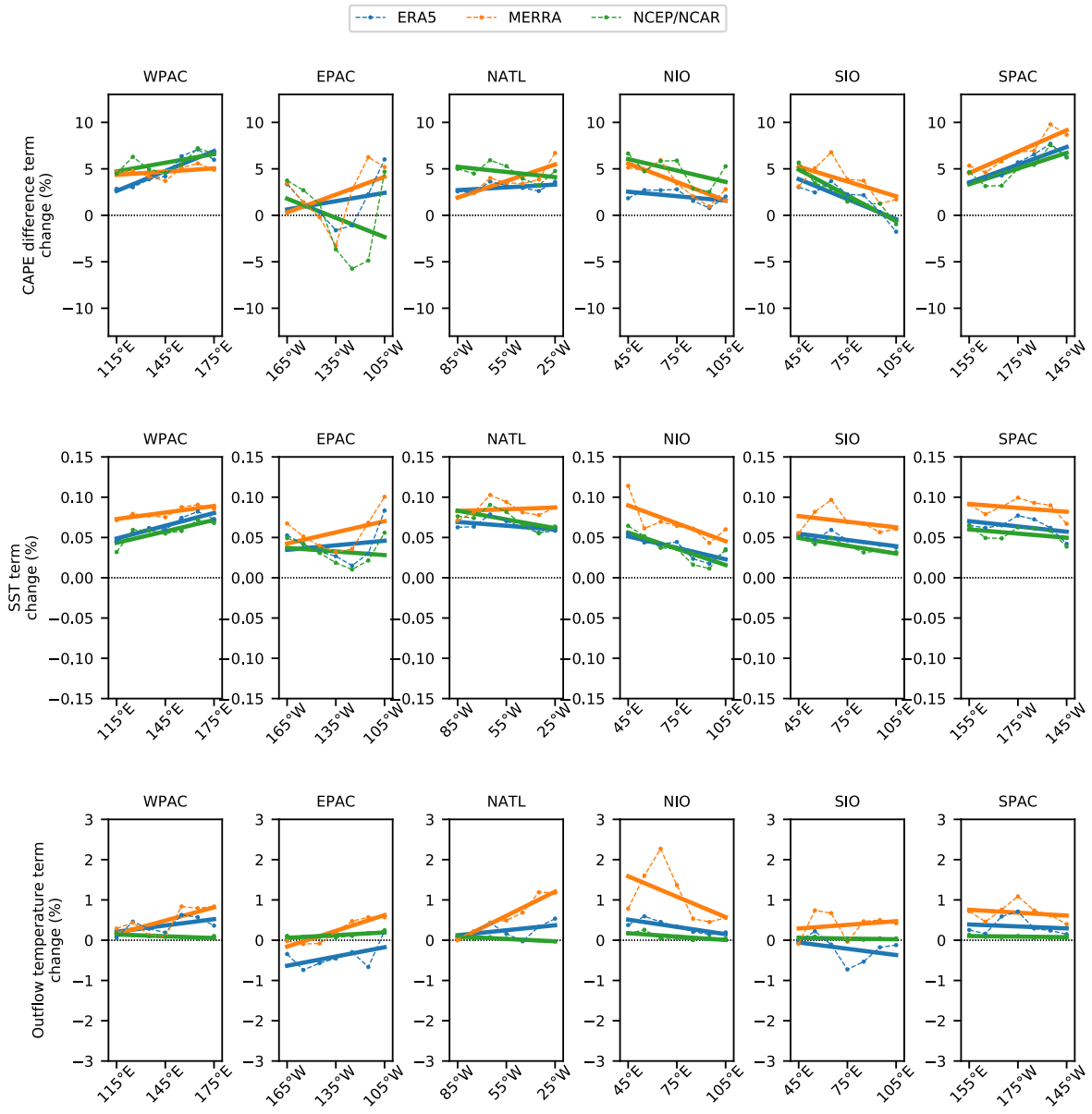

Fig. S5. As in Fig. S4, but for the three terms in Equation (1) for the potential intensity calculation. a-f, convective available potential energy (CAPE) difference term $\sqrt{(\boldsymbol{CAPE_s - CAPE})}$. g-l, the sea surface temperature (SST) term $\sqrt{\boldsymbol{T_s}}$. m-r, the outflow temperature term $\sqrt{\frac{\boldsymbol{1}}{\boldsymbol{T_o}}}$. Note that the y-axis scales are difference amongst the terms.

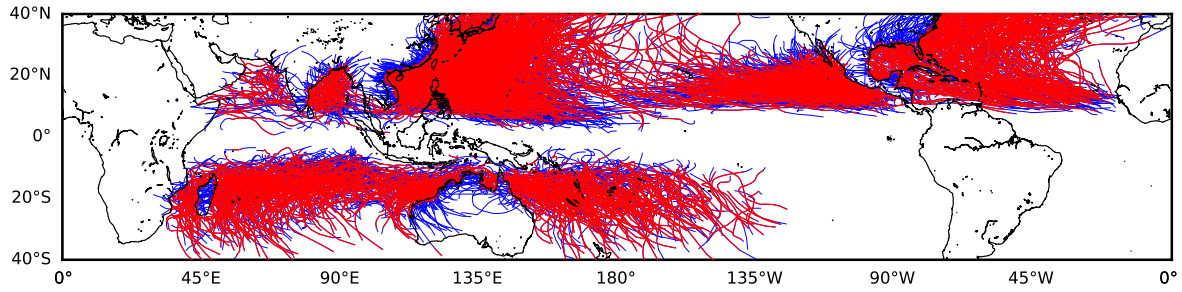

Fig. S6. The full tracks of tropical cyclones with the lifetime maximum intensity of at least 34 knots (blue lines) and the selected tracks used in our analysis (red lines) over the period 1982-2018.

Table S1. Linear trends, by region, of annual-mean distance (km) to land of the locations of life-time maximum intensity (LMI), fraction (%) of annual tropical cyclones entering coastal regions, and time fraction (%) of annual-mean life span spent in coastal regions, as shown in Fig. 1. The trends after removing the ENSO, ENSO Modoki (ENSO-M) and PDO contributions are also calculated for all three trends. The statistics in the WPAC and NATL are also extended to the period 1950-2018 in parentheses. Statistical significance is indicated in bold at the 95% confidence interval.

	Global	NHEM	SHEM	WPAC	EPAC	NATL	NIO	SIO	SPAC
LMI location to land	**-32±31**	-25±40	**-50±44**	-43±65 (-12±24)	-28±57	29±55 (**23±19**)	24±35	-26±54	-56±81
ENSO removed	–	-24±28	**-45±42**	-41±48 (**-24±19**)	-27±51	29±53 (18±19)	24±33	-22±53	-48±78
ENSO-M removed	–	-29±34	**-50±44**	-49±59 (-12±22)	-33±53	25±53 (**23±19**)	22±32	-25±53	-58±79
PDO removed	–	-5±37	**-51±44**	-6±56 (**-21±20**)	-15±56	27±55 (**22±19**)	27±35	-27±54	-53±80
Fraction of annual number	**2.2±1.9**	**2.5±2.2**	1.3±3.2	**2.8±2.7** (1.0±1.2)	4.0±4.5	0.2±4.6 (-0.4±1.7)	-2.6±5.7	1.3±4.3	-0.4±4.3
ENSO removed	–	**2.5±1.9**	0.9±3.1	**2.8±2.7** (**1.3±1.1**)	4.0±4.4	0.2±4.2 (0.0±1.6)	-2.6±5.7	0.9±4.2	-0.8±4.1
ENSO-M removed	–	**2.6±2.1**	1.2±3.2	**2.8±2.7** (1.0±1.2)	**4.3±4.3**	0.6±4.3 (-0.4±1.6)	-2.4±5.7	1.2±4.2	-0.3±4.3
PDO removed	–	2.0±2.1	1.2±3.2	2.0±2.6 (**1.3±1.1**)	4.3±4.5	0.1±4.6 (-0.3±1.7)	-2.1±5.7	1.1±4.3	-0.6±4.3
Time fraction of life span	**2.1±1.2**	**2.1±1.6**	**2.1±1.9**	1.5±1.9 (**1.0±0.7**)	**3.2±2.4**	0.3±3.0 (0.4±1.1)	-2.0±4.7	1.5±2.5	2.4±3.2
ENSO removed	–	**2.0±1.2**	**1.9±1.8**	1.5±1.6 (**1.3±0.7**)	**3.2±2.3**	0.3±2.7 (0.7±1.0)	-2.0±4.5	1.3±2.5	2.2±3.2
ENSO-M removed	–	**2.2±1.5**	**2.1±1.9**	1.7±1.8 (**1.0±0.7**)	**3.3±2.3**	0.5±2.9 (0.4±1.0)	-1.6±4.3	1.4±2.5	2.4±3.2
PDO removed	–	1.3±1.5	**2.0±1.9**	0.7±1.7 (**1.2±0.7**)	**3.0±2.4**	-0.3±2.9 (0.5±1.0)	-2.3±4.5	1.4±2.5	2.3±3.2

Table S2. Linear slope of the trends, by region, of the frequency of annual tropical cyclones entering coastal regions by changing the distance-to-land threshold from 200 km to 2000 km at every 100-km interval (see Fig. 2). The fitted slope represents the change in the trends with a unit of cyclone count per decade per 1000 km to land. The slope of trends after removing the ENSO, ENSO Modoki (ENSO-M) and PDO contributions are also calculated. Statistical significance is indicated in bold at the 95% confidence interval.

	Global	NHEM	SHEM	WPAC	EPAC	NATL	NIO	SIO	SPAC
Slope	**-1.0±0.1**	**-0.5±0.1**	**-0.5±0.1**	**-0.6±0.1**	**-0.6±0.3**	**0.7±0.2**	0.0±0.0	**-0.4±0.1**	0.0±0.1
ENSO removed	–	**-0.5±0.1**	**-0.4±0.1**	**-0.6±0.1**	**-0.6±0.3**	**0.7±0.2**	0.0±0.0	**-0.4±0.1**	0.0±0.1
ENSO-M removed	–	**-0.6±0.1**	**-0.5±0.1**	**-0.7±0.1**	**-0.7±0.4**	**0.7±0.2**	0.0±0.0	**-0.4±0.1**	-0.0±0.1
PDO removed	–	**-0.2±0.1**	**-0.4±0.1**	**-0.4±0.1**	**-0.3±0.2**	**0.5±0.1**	0.0±0.0	**-0.4±0.1**	-0.0±0.1

Table S3. Fraction (%) of global annual tropical cyclones entering coastal regions as in Fig. 1b, linear slope of the trends of the frequency of global annual tropical cyclones entering coastal regions by changing the distance-to-land threshold as in Fig. 2, and the epochal mean westward shift of global tropical cyclone locations (degree longitude) as in Table 1. The trends based on the best track provided by the U.S. agencies are compared with the results by (1) removing the short-lived cyclones with intensity above tropical-storm strength for less than two days, and (2) using the global best track data taken from the World Meteorological Organization (WMO) agencies. Statistical significance is indicated in bold at the 95% confidence interval.

	U.S. agencies	U.S. agencies without short-lived cyclones	WMO agencies
Fraction of annual cyclones	**2.2±1.9**	**1.8±1.8**	**2.5±1.9**
Linear slope of the trends	**-1.0±0.1**	**-0.9±0.1**	**-0.6±0.2**
Westward shift	**0.8±0.2**	**1.0±0.2**	**0.8±0.2**

Table S4. As in Table 1, but for the genesis location where a tropical cyclone is identified as a tropical storm for the first time, zonal and meridional translation velocity of tropical cyclones, and tropical cyclone duration. Positive zonal and meridional velocities represent westward and poleward displacements, respectively. Statistical significance is indicated in bold at the 95% confidence interval.

	Global	NHEM	SHEM	WPAC	EPAC	NATL	NIO	SIO	SPAC
Genesis westward (degree longitude)	+0.8±1.4	+0.8±1.5	+0.8±3.2	+1.1±2.0	–0.1±2.7	–1.2±4.0	+1.0±3.3	+1.8±4.2	+0.2±4.4
Genesis poleward (degree latitude)	**+0.4±0.4**	+0.4±0.5	+0.4±0.5	+0.6±0.8	**+0.7±0.4**	0.0±1.5	–0.4±1.2	+0.1±0.6	**+1.0±0.8**
Cyclone velocity westward ($m\ s^{-1}$)	0.0±0.1	**–0.1±0.1**	**+0.1±0.1**	**+0.2±0.1**	**–0.5±0.1**	**+0.4±0.2**	+0.1±0.2	**–0.5±0.1**	**+0.4±0.1**
Cyclone velocity poleward ($m\ s^{-1}$)	**+0.2±0.1**	**+0.1±0.1**	**+0.3±0.1**	**+0.2±0.1**	**+0.1±0.1**	**–0.3±0.1**	**–0.4±0.1**	**+0.2±0.1**	**+0.3±0.1**
Duration (hour)	–8±122	–25±84	–11±99	–8±121	–14±45	+3±27	+1±52	–6±81	–21±91

Table S5. As in Table 1, but for the statistics with only PDO neutral years. NHEM (1984, 1986, 1988, 1989, 1990, 1991, 1996, 2002, 2004, 2007, 2009, 2017 and 2018). SHEM (1982, 1992, 1993, 1995, 1997, 1999, 2001, 2002, 2007, 2013, 2018).

	Global	NHEM	SHEM	WPAC	EPAC	NATL	NIO	SIO	SPAC
Westward	**+2.2±0.4**	**+1.7±0.5**	**+3.8±0.7**	-0.5±0.6	**+5.5±1.0**	**+1.0±0.8**	**+6.5±0.8**	**+6.1±0.8**	–0.2±0.9
Poleward	**+0.3±0.2**	**+0.2±0.2**	**+0.5±0.4**	**+0.6±0.4**	**+0.3±0.3**	**–0.4±0.4**	0.0±0.4	**+1.0±0.5**	0.0±0.8